Improved performances of 2. 6 μm $In_{0.83} Ga_{0.17}$ As/InP photodetectors on digitally–graded metamorphic pseudo–substrates

SHI Yan–Hui[1 2]　　YANG Nan–Nan[1 2]　　MA Ying–Jie[1 3 4]　　GU Yi[1 3 4 *]　　CHEN Xing–You[1]
GONG Qian[1]　　ZHANG Yong–Gang[1 3 4]

（1. State Key Laboratory of Functional Materials for Informatics　Shanghai Institute of Microsystem and Information Technology
Chinese Academy of Sciences　Shanghai 200050　China；
2. University of Chinese Academy of Sciences　Beijing 100049　China；
3. State Key Laboratory of Transducer Technology　Shanghai Institute of Technical Physics
Chinese Academy of Sciences　Shanghai 200083　China；
4. Key Laboratory of Infrared Imaging Materials and Detectors　Shanghai Institute of Technical Physics
Chinese Academy of Sciences　Shanghai 200083　China）

Abstract：Impacts of the total period number for the $In_{0.83} Al_{0.17}$ As/$In_{0.52} Al_{0.48}$ As digitally–graded metamorphic buffer（DGMB）on the performances of 2. 6 μm $In_{0.83} Ga_{0.17}$ As photodiodes（PDs）have been investigated. An in–crease of the total period number from 19 to 38 for the $In_{0.83} Al_{0.17}$ As/$In_{0.52} Al_{0.48}$ As DGMB with the same thickness has shown improved crystal qualities for the $In_{0.83} Ga_{0.17}$ As/$In_{0.83} Al_{0.17}$ As photodiode layers grown on such pseudo–substrates. An increased strain relaxation degree up to 99. 8%　a reduced surface roughness　enhanced photolumi–nescence intensities as well as photo responsivities　and suppressed dark currents are observed simultaneously for the $In_{0.83} Ga_{0.17}$ As photodiode on the DGMB with a period number of 38. These results suggest that with more peri–ods　DGMB can restrain the transmission of the threading dislocations more efficiently and reduce the residual de–fect density.

Key words：digital–grading　metamorphic buffer InGaAs　photodetectors
PACS：81. 05. Ea　81. 15. Hi

2. 6 μm $In_{0.83} Ga_{0.17}$ As/InP

1 2　　　　　1 2　　　　　1 3 4　　　　　1 3 4 *　　　　　1　　　　　1　　　　　1 3 4

（1.　　　　　　　　　　　　　　　　　　　　　　　　　200050；
2.　　　　　　　　100049；
3.　　　　　　　　　　　　　200083；
4.　　　　　　　　　　　200083）

：　　　　$In_{0.83} Al_{0.17}$ As/$In_{0.52} Al_{0.48}$ As　　　　　　　　　（DGMB）　　　　2. 6 μm
$In_{0.83} Ga_{0.17}$ As　　　　　　　　　.　　　　　　　　　　　　　　　　　　　　InP
　　$In_{0.83} Al_{0.17}$ As/$In_{0.52} Al_{0.48}$ As DGMB　　　　　　19　　　38　　　　　　$In_{0.83} Ga_{0.17}$ As/$In_{0.83}$
$Al_{0.17}$ As　　　　　　　　　　　　　.　　　　　　38　DGMB　　　　$In_{0.83} Ga_{0.17}$
As　　　　　　　　　　　99. 8%
　　　　　　.　　　　　　　　　　DGMB
　　　.

Introduction

As parts of the atmospheric windows the 2 ~ 3 μm short wave infrared (SWIR) band has found significant applications in remote sensing spectral imaging earth observation night vision *et al.* [1-3]. Workhorse detectors in the SWIR band are the HgCdTe pin the InSb pin and the wavelength‑extended Indium‑rich $In_x Ga_{1-x} As/InP$ ($x > 0.53$) pin photodiodes. Considering the uniformity issues for HgCdTe films and the difficulties in both growth and processing for antimonies the Indium‑rich $In_x Ga_{1-x} As$ ($x > 0.53$) photodetectors (PDs) and focal plane arrays (FPAs) have now become increasingly important in this particular wavelength range for their excellent optical and electrical performances [4]. Different from the communication applications that emphasize on the high response speed for the PDs the dark current performances are more important for the 2 ~ 3 μm PDs and FPAs used for remote sensing applications. In general the diffusion current dominates the dark current at around room temperature for the metamorphic $In_x Ga_{1-x} As$ pin PDs whereas at lower temperatures the generation‑recombination (G‑R) and the trap‑assisted tunneling (TAT) currents are the dominant sources [3-6]. The high threading dislocation densities (TDDs) as well as the concomitant high dark current levels have been the main drawbacks for Indium‑rich $In_x Ga_{1-x} As$ PDs due to lacking of a lattice‑matched substrate [7]. The linearly graded $In_x Al_{1-x} As$ and $InAs_x P_{1-x}$ buffer structures have been well‑developed as pseudo‑substrates for the wavelength‑extended $In_x Ga_{1-x} As$ PDs with cutoff wavelengths beyond 1. 7 μm [8][9]. However owing to the threading nature of the misfit dislocations the residual dislocation density remains high even after epitaxial of buffer layers up to several microns. Different buffer schemes such as the step‑graded [10][11] the staircase graded [12] the superlattice [13][14] and the continuously graded buffers [15][16] have been proposed and demonstrated showing decreased defect densities. Recently a modified buffer scheme namely the digitally‑graded metamorphic buffer (DGMB) that contains multi‑period $In_{0.83} Al_{0.17} As/In_{0.52} Al_{0.48} As$ layers with thicknesses varied in a digital alloy pattern was proposed on InP substrates in which the preferentially dislocation nucleation and the blocking of TD transmission near the $In_{0.83} Al_{0.17} As/In_{0.52} Al_{0.48} As$ interfaces were observed [17]. However impacts of the structural parameters for the DGMB pseudo‑substrate such as the period number the total thickness the growth temperatures and the growth rates on the performances of the metamorphic $In_{0.83} Ga_{0.17} As/InP$ PDs have not been investigated. Given that the TDD of the $In_{0.83} Ga_{0.17} As$ light absorption layer is directly determined by the strain relaxation degree in the metamorphic buffer region investigation on the detector characteristics with different DGMB parameters would help understand the defect evolvement behavior in DGMB and achieve better performances.

In this work the impacts of period number of $In_{0.83} Al_{0.17} As/In_{0.52} Al_{0.48} As$ DGMB on the performances of the $In_{0.83} Ga_{0.17} As/InP$ PDs are experimentally analyzed. Compared with a reference $In_{0.83} Ga_{0.17} As$ PD grown on a DGMB pseudo‑substrate with a period number of 19 (referred to as PD‑1) the surveyed performances for the PD with the same thickness of the DGMB region but doubled period number (referred to as PD‑2) are notably improved. The material characterizations as well as device characteristics are discussed in detail.

1 Experimental details

Both PD wafers were grown in a gas source molecular beam epitaxy (GSMBE) system (VG Semicon V80H) on heavily doped n$^+$ InP (001) substrates. Device structures are identical for both PDs except for the total period numbers for the DGMB region. The growth started sequentially from a 0. 2‑μm‑thick InP a 0. 1‑μm‑thick $In_{0.52} Al_{0.48} As$ a 1. 9‑μm‑thick $In_y Al_{1-y} As$ DGMB region and a 0. 4‑μm‑thick $In_{0.83} Al_{0.17} As$ layers which were all n doped to 1×10^{18} cm^{-3} with silicon. After that a 1. 6‑μm‑thick n$^-$ doped (silicon 3×10^{16} cm^{-3}) $In_{0.83} Ga_{0.17} As$ absorption layer was grown. Finally a 0. 6‑μm‑thick p$^+$ $In_{0.83} Al_{0.17} As$ cladding layer heavily doped with beryllium to 5×10^{18} cm^{-3} was grown to finish the whole structure [18]. The total thicknesses for the DGMB regions were kept the same (1. 9 μm) while the total period numbers were 19 (PD‑1) and 38 (PD‑2) respectively. For PD‑1 the thickness ratio between $In_{0.52} Al_{0.48} As$ and $In_{0.83} Al_{0.17} As$ in each period were gradually varied in opposite directions from 19:1 to 1:19. The corresponding thicknesses for the $In_{0.52} Al_{0.48} As$ and $In_{0.83} Al_{0.17} As$ in each period were therefore varied from 95 and 5 nm to 5 and 95 nm respectively. Similarly those of PD‑2 were from 38:1 to 1:38 and the corresponding thicknesses were varied from 48. 7 and 1. 3 nm to 1. 3 and 48. 7 nm respectively. After growth 200‑μm‑diameter mesa PDs were fabricated. After $Si_3 N_4$ passivation [19] metal deposition liftoff and thermal annealing the PDs were diced into chips for measurements. Fig. 1 illustrates the schematic structures for both PDs 1 and 2.

The crystalline qualities and the surface properties for both wafers were carried out by using X‑ray diffraction (XRD) and atomic force microscopy (AFM). XRD reciprocal space map (RSM) measurements were characterized by using a Philips X’pert MRD high resolution X‑ray diffractometer equipped with a four‑crystal Ge (220) monochromator. AFM measurements were characterized by using a Veeco Nanoscope Ⅲ Atomic Force Microscope System. The optical quality of the samples was further evaluated by photoluminescence (PL) measurements. The PL spectra were acquired by using a Thermo Scientific

3

SHI Yan-Hui *et al*: Improved performances of 2.6 μm In$_{0.83}$Ga$_{0.17}$As/InP photodetectors
on digitally-graded metamorphic pseudo-substrates

277

Nicolet iS50 Fourier transform infrared (FTIR) spectrometer adopting a home-made optical accessory. The wafers were mounted onto a continuous-flow helium cryostat to control temperature while a 532 nm diode pumped solid state laser was used as the excitation source. The spectral response of the PDs was carried out by using the FTIR setup in the temperature range from 300 K to 77 K where the output signals from the PDs were fed into the preamplifier of the spectrometer. In the measurement the packaged chips with a diameter of 200 μm were installed in a liquid-nitrogen Dewar to control the temperature. The temperature-dependent behaviors of the dark currents were carried out by using a cryogenic probe station connected to a HP4156A precise semiconductor analyzer.
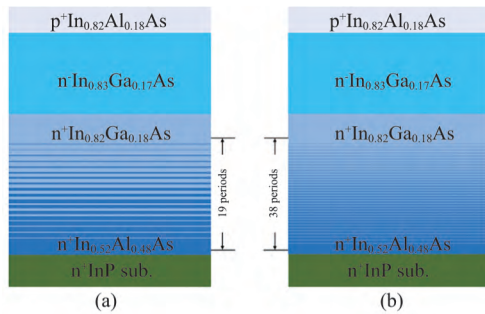

Fig. 1 Schematic illustrations for the detector structures for the (a) PD-1 and (b) PD-2
图 1 (a) PD-1 (b) PD-2

2 Results and discussion

Fig. 2(a) and (b) show the AFM images with 40 × 40 μm^2 surface areas for the PD samples respectively. Both samples exhibit a closely-packed oval structure elongated along 110. Undulated ripples along 110 were clearly observed for both samples which are attributed to the generation of periodic strain field during grading and the associated energetic favorable strain relaxation along 110 [20]. The AFM measurements indicate that the root-mean-square (RMS) roughness for the PD-2 is 9.1 nm lower than that of 9.7 nm for the PD-1. Such slightly reduced RMS roughness suggests a better crystallinity for the metamorphic In$_{0.83}$Ga$_{0.17}$As layer on the 38 periods DGMB pseudo-substrate.

To determine the structural properties of the samples the relaxation degrees and the residual strain of the wafers were carried out by the XRD RSM measurements along both symmetric (004) and asymmetric (115) planes as shown in Fig. 3. The vertical and horizontal axes represent the reciprocal lattice in the 001 (q_y) and 110 (q_x) directions. Apart from the InP substrate peak (denoted by S) two epitaxial peaks were identified in all the mapping figures denoted by L1 and L2 respectively. The two relatively strong epitaxial peaks are corresponded to the relaxed In$_{0.83}$Ga$_{0.17}$As absorption layer (L1) and the relaxed In$_{0.83}$Al$_{0.17}$As cap layer (L2) [21] respectively. In the (004) RSM for the sample
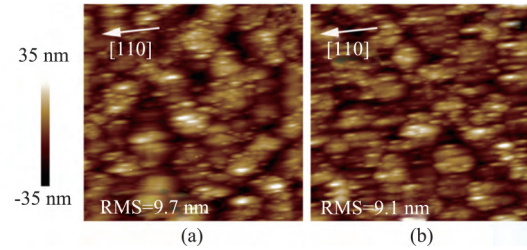

Fig. 2 AFM images of the surface morphologies for samples (a) PD-1 and (b) PD-2. Size: 40 × 40 μm^2
图 2 (a) PD-1 (b) PD-2 AFM
. :40 × 40 μm^2

ple PD-2 the location of peak diffraction intensity for the epitaxial layers is centered along the drawn vertical line through the center of the substrate indicate the PD-2 has less tilting angle than that of the PD-1. For the asymmetric (115) reflections the full relaxation and pseudomorphic lines regarding the substrate were drawn for reference. The corresponding strain relaxation parameters were also extracted as listed in Table 1. The degree of strain relaxation for PD-2 is 99.8% higher than that of 94.8% for PD-1 again suggests that the epitaxial layers relaxed more efficiently in the sample with more periods in the DGMB.

Table 1 Strain relaxation parameters extracted from the XRD measurements
表 1 XRD

Sample	Degree of relaxation (%)	Tilting Angle (°)	Parallel Mismatch (%)
PD-1	94.8	0.175 7	0.884
PD-2	99.8	0.011 4	1.911

Cross-sectional transmission electron microscopy (XTEM) measurements were also conducted to further investigate the generation and the evolution of the TDs along the growth directions for both PDs as shown in Fig. 4. Interfaces between In$_{0.52}$Al$_{0.48}$As/In$_{0.82}$Al$_{0.17}$As in the DGMB regions could be clearly observed for both PDs. However the TDDs in the upper In$_{0.83}$Ga$_{0.17}$As light absorption layers could not be accurately determined given that the relatively small field of view in the TEM measurements. While the observed numbers of macroscopic dislocation defects from both Fig. 4(a) and (b) were in the same order of magnitude the dislocation nucleation behaviors in the DGMB regions for both PDs were significantly different as indicated by the white arrows in Fig. 4(c) and (d) for PD-1 and PD-2 respectively. The dislocations exhibited preferentially nucleation nature near the interfaces between In$_{0.52}$Al$_{0.48}$As/In$_{0.82}$Al$_{0.17}$As and the number of such nucleation was notably higher for PD-2 with 38 periods than that for PD-1. In addition these dislocations were short and pinned between interfaces which demonstrates that the effectiveness of the blocking effect of the TDs in the DGMB structure. Such increased number of dislocations in the DGMB region for PD-2 also suggested that the increased number of periods in the DGMB region would lead to
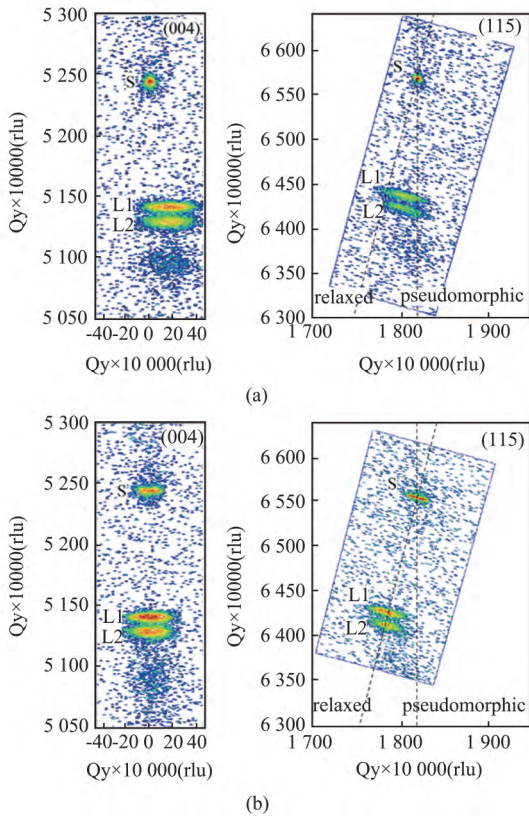
Fig. 3 Symmetric (004) and asymmetric (115) RSMs for the samples of (a) PD-1 and (b) PD-2

图 3 (a) PD-1 (b) PD-2 的对称 (004) 和非对称 (115) RSM 图

more effective strain relaxation and thus lower residual strain and better material quality. These results were also consistent with the measured lower strain relaxation degree for the 38-period wafer from the XRD measurements, as listed in Table. 1.
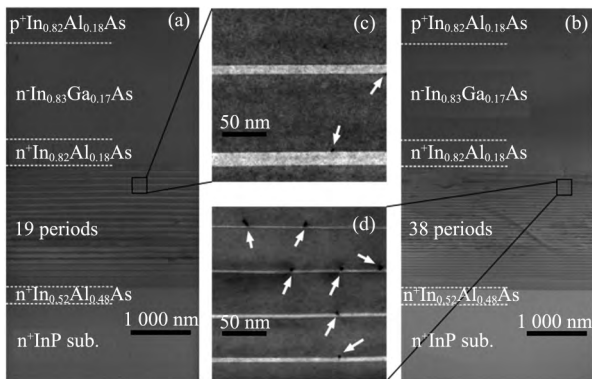

Fig. 4 XTEM images of the detector structures for the (a) PD-1 and (b) PD-2

图 4 (a) PD-1 (b) PD-2 探测器结构的 XTEM 图

Optical properties of the PDs were carried out by using PL measurements at 100, 200, and 300 K, as shown in Fig. 5(a). The excitation laser power is about 0.3 W with a spot diameter of around 1.5 mm. The peaks correspond to the $In_{0.83}Ga_{0.17}As$ absorption layers showed blueshifts with the decrease of temperature. With increasing temperature, an increasing number of photogenerated carriers tend to relax via the non-radiative recombination channels such as the Auger and the defect states-related trapping processes, leads to the attenuation of the PL intensity. The PL intensities for the PD-2 are higher than that for the PD-1 over the whole measured temperature range suggests that the amount of non-radiative recombination centers in the $In_{0.83}Ga_{0.17}As$ absorption layer of PD-2 was reduced compared to that of PD-1. Such a reduction indicates the transmission of threading dislocations is suppressed by the increased number of $In_{0.83}Al_{0.17}As/In_{0.52}Al_{0.48}As$ interfaces in PD-2 and thus a lower residual dislocation density is realized for PD-2.

Fig. 5(b) shows the Arrhenius plots of the integrated PL intensities for both samples. The data are well fitted by using an bi-exponential activation energy model formulated by $I(T) = \alpha \left[1 + C_1 \exp(-E_1/k_B T) + C_2 \exp(-E_2/k_B T) \right]^{-1}$ where T is the temperature, $I(T)$ is the integrated PL emission intensity, α, C_1 and C_2 are fitting parameters, k_B is Boltzmann's constant, E_1 and E_2 are the thermal activation energies in the higher ($T > 180$ K) and the lower ($T < 180$ K) temperature ranges respectively [22, 23]. The E_1 in the higher temperature range generally corresponds to the detrapping energy of the carriers that are trapped by the defect levels. The E_1 of PD-2 (99.5 meV) is higher than that of PD-1 (43.4 meV) in the higher temperature range, which could be attributed to the lower residual strain and the lower defect density in PD-2. Similarly, at lower temperatures, the E_2 of PD-2 (12.3 meV) is also higher than that of PD-1 (5.4 meV), which could be explained by the same origin. Given that the smaller thermal activation energies mean that thermally activated nonradiative recombination can easily occur in the sample of PD-1, which is considered due to the relatively high strain of $In_{0.83}Ga_{0.17}As$ layers [24].
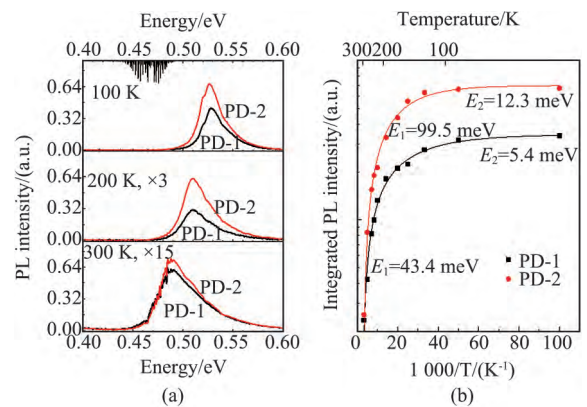

Fig. 5 (a) PL spectra for the PD-1 and PD-2 at 100, 200, and 300 K. (b) The Arrhenius plots of the integrated PL intensities for both PDs. The fitted E_1 and E_2 are indicated

图 5 (a) PD-1 和 PD-2 在 100, 200, 300 K 的 PL 谱. (b) 两个 PD 的 PL 积分强度的 Arrhenius 图. 图中标出了拟合的 E_1 和 E_2

The lower residual defect density for the 38 period

3
SHI Yan-Hui *et al*: Improved performances of 2.6 μm In$_{0.83}$Ga$_{0.17}$As/InP photodetectors
on digitally-graded metamorphic pseudo-substrates
279

DGMB structure was further verified from the perform-ances of PDs grown on such pseudo-substrates. The spectra responsivities and the dark currents of the PDs were measured for mesa-type devices with a diameter of 200 μm. Fig. 6 shows the temperature-dependent spec-tral responsivities for both PDs ranging from 77 to 300 K acquired by using a FTIR setup [25]. The same peak and 50% cutoff wavelengths of 2.23 and 2.57 μm respec-tively at 300 K were observed for both PDs. The abso-lute spectral responsivity values were scaled using the re-sponsivity at 2.0 μm obtained from current-voltage (I-V) measurements using a 2.0 μm semiconductor laser with an accurately calibrated power. PD-2 has shown a slightly higher responsivity of 1.13 A/W at 2.23 μm than that for PD-1 (1.07 A/W) at 300 K indicating that a lower residual defect density and an associated lon-ger carrier lifetime are achieved for PD-2. Meanwhile the 50% cutoff wavelengths of both PDs blueshift to 2.35 μm at 77 K due to the increased band gap energy. To ensure the reproducibility of data the data were measured on more than 5 devices and averaged for each sample.
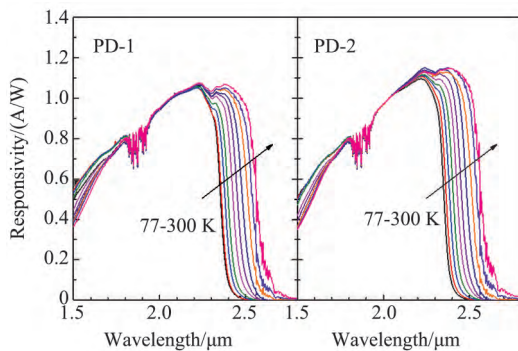

Fig. 6   The zero-bias temperature-dependent spectral responsivities for both PDs with the same mesa diameter of 200 μm
6   PD (200 μm)

The temperature-dependent dark *I-V* curves for both PDs ranging from 77 ~ 300 K were shown in Fig. 7. The dark currents for PD-2 were almost the same as that for PD-1 in a higher temperature range of $T > 225$ K where-as decrease more rapidly with decreasing the tempera-ture. The 300 K dark currents at a reverse bias of -0.1 V for PD-1 and PD-2 are 2.76 and 2.02 μA respectively. As the temperature decreased to 77 K the −0.1 V dark current for PD-1 is 670 pA while for PD-2 it decreases sharply by more than an order of magnitude to 14.6 pA.

The Arrhenius plots of the dark currents at -10 mV for the two PDs are shown in Fig. 8. An activation ener-gy E_a can be fitted from $I_d \propto \exp(-E_a/k_B T)$ where I_d represents the −10 mV dark current. It is found that in the high-temperature range of $T > 175$ K the extracted E_a is 0.39 eV for PD-2 near to the band gap of the In$_{0.83}$Ga$_{0.17}$As absorption layer represents that the dark current is dominant by the diffusion process above 175 K for PD-2 [26]. With decreasing the temperature the slope declined indicates that the TAT currents are playing increasingly important roles for the total I_d. For PD-1
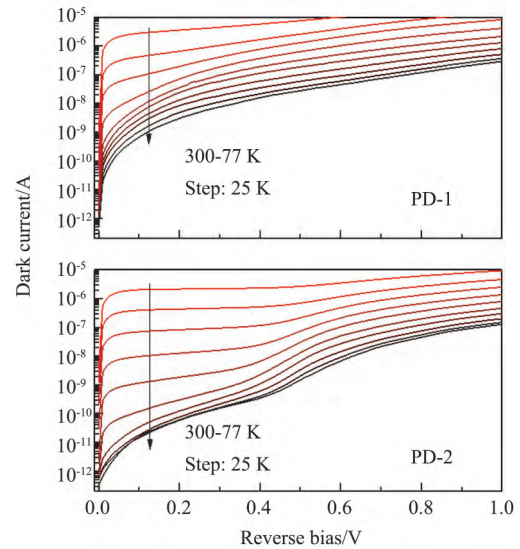

Fig. 7   Temperature-dependent dark I-V curves for both PDs from 77 to 300 K
7   PD   I-V   :
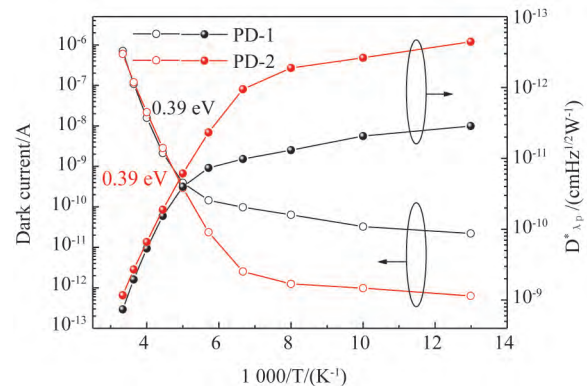77-300 K

Fig. 8   Arrhenius plots of the dark currents under −10 mV and the peak detectivity $D^*_{\lambda p}$ versus reciprocal temperatures for both PD-1 (black points) and PD-2 (red points)
8   PD-1(   )   PD-2(   )   -10 mV
$D^*_{\lambda p}$ Arrhenius

the diffusion current dominant temperature range was $T > 225$ K indicates that the residual dislocation defect den-sity is higher for PD-1. Below 200 K the I_d for both PDs saturated which are related with the shallow defect states. PD-2 revealed significantly improved dark currents of a-bout two orders of magnitude lower at 77 K with respect to PD-1 indicates that the defect-related TAT leakages are significantly reduced.

To further evaluate the performances of the PDs the responsivity and noise measurements were measured u-sing a calibrated blackbody at 900 K. The peak detectiv-ity $D^*_{\lambda p}$ were also acquired and plotted in Fig. 8. The temperature dependency of $D^*_{\lambda p}$ have exhibited similar trends as compared with that of I_d. At 300 K PD-1 showed slightly lower $D^*_{\lambda p}$ compared with PD-2 which

were 7.39×10^8 and 1.17×10^9 cmHz$^{1/2}$/W respectively. As the temperature decreases the $D^*_{\lambda p}$ for PD-2 climbed much faster than that for PD-1. The 77 K value for PD-2 was 4.42×10^{12} cmHz$^{1/2}$/W more than an order of magnitude higher than that for PD-1 (2.86×10^{11} cmHz$^{1/2}$/W). These results again demonstrate the better material quality for PD-2 with more periods in the DGMB region.

3 Conclusions

In conclusion we have investigated the performances for two 2.6 μm metamorphic In$_{0.83}$Ga$_{0.17}$As/InP PDs with different periods of DGMB structure. The characteristics of both PDs were investigated and compared by using AFM XRD TEM PL the response spectra and the dark current measurements. The PL intensities are improved and the dark current decreased by about two orders of magnitude for an In$_{0.83}$Ga$_{0.17}$As PD grown on a 38 period In$_{0.83}$Al$_{0.17}$As/In$_{0.52}$Al$_{0.48}$As pseudo-substrate in comparison to a reference PD grown on a 19 period DGMB. With more periods DGMB can restrain the transmission of threading dislocations more efficiently leading to a lower residual defect density. These results suggest that by extensive optimization on the structural parameters for the DGMB pseudo-substrate the residual defect density of active layers can be further reduced and the device performances can be significantly improved.

Acknowledgments

References

1 Frankenberg C Aben I Bergamaschi P *et al*. Global column-averaged methane mixing ratios from 2003 to 2009 as derived from SCIAMACHY: Trends and variability J. *J Geophys Res-Atmos* 2011 **116**: D04302.

2 Parker R Boesch H Cogan A *et al*. Methane observations from the Greenhouse Gases Observing SATellite: Comparison to ground-based TCCON data and model calculations J. *Geophys. Res. Lett.* 2011 **38**: L15807.

3 Hoogeveen R W M van der A R J Goede A P H. Extended wavelength InGaAs infrared (1.0-2.4 μm) detector arrays on SCIAMACHY for space-based spectrometry of the Earth atmosphere J. *Infrared Phys. Technol.* 2001 **42**(1): 1-16.

4 Zhang Y G Gu Y Chen X Y *et al*. An effective indicator for evaluation of wavelength extending InGaAs photodetector technologies J. *Infrared Phys. Technol.* 2017 **83**: 45-50.

5 Linga K R Olsen G H Ban V S *et al*. Dark Current Analysis and Characterization of In$_x$Ga$_{1-x}$As/InAs$_y$P$_{1-y}$ Graded Photodiodes with $x >$ 0.53 for Response to Longer Wavelengths (> 1.7 μm) J. *J. Lightwave Technol.* 1992 **10**(8): 1050-1055.

6 Li C Zhang Y G Wang K *et al*. Distinction investigation of InGaAs photodetectors cutoff at 2.9 μm J. *Infrared Phys. Technol.* 2010 **53**(3): 173-176.

7 Hudait M K Lin Y Ringel S A. Strain relaxation properties of InAs$_y$P$_{1-y}$ metamorphic materials grown on InP substrates J. *J. Appl. Phys.* 2009 **105**(6): 12.

8 Zhang Y G Gu Y Wang K *et al*. Properties of gas source molecular beam epitaxy grown wavelength extended InGaAs photodetector structures on a linear graded InAlAs buffer J. *Semicond. Sci. Technol.* 2008 **23**(12): 125029.

9 D'Hondt M Moerman I Van Daele P *et al*. Influence of buffer layer and processing on the dark current of 2.5 μm-wavelength 2%-mismatched InGaAs photodetectors J. *IEE Proc. -Optoelectron.* 1997 **144**(5): 277-282.

10 Shang X Z Wu S D Liu C *et al*. Low temperature step-graded InAlAs/GaAs metamorphic buner layers grown by molecular beam epitaxy J. *J. Phys. D: Appl. Phys.* 2006 **39**(9): 1800-1804.

11 Lee D Park M S Tang Z *et al*. Characterization of metamorphic In$_x$Al$_{1-x}$As/GaAs buffer layers using reciprocal space mapping J. *J. Appl. Phys.* 2007 **101**(6): 8.

12 Chen E B Paine D C Uppal P N *et al*. Surface morphology evolution in highly mismatched Sb-graded buffer layers on GaAs J. *Appl. Phys. Lett.* 2001 **78**(16): 2345-2347.

13 Pease E A Dawson L R Vaughn L G *et al*. 2.5-3.5 μm optically pumped GaInSb/AlGaInSb multiple quantum well lasers grown on AlInSb metamorphic buffer layers J. *J. Appl. Phys.* 2003 **93** (6): 3177-3181.

14 Wada M Hosomatsu H. Wide wavelength and low dark current latticemismatched InGaAs/InAsP photodiodes grown by metalorganic vaporphase epitaxy J. *Appl. Phys. Lett.* 1994 **64**(10): 1265-1267.

15 Lin G R Kuo H C Lin C K *et al*. Ultralow leakage In$_{0.53}$Ga$_{0.47}$As p-i-n photodetector grown on linearly graded metamorphic In$_x$Ga$_{1-x}$P buffered GaAs substrate J. *IEEE J. Quantum Electron.* 2005 **41** (6): 749-752.

16 Choi H Jeong Y Cho J *et al*. Effectiveness of non-linear graded buffers for In(Ga Al)As metamorphic layers grown on GaAs (001) J. *J. Cryst. Growth* 2009 **311**(4): 1091-1095.

17 Ma Y J Zhang Y G Chen X Y *et al*. A versatile digitally-graded buffer structure for metamorphic device applications J. *J. Phys. D: Appl. Phys.* 2018 **51**(14): 8.

18 Zhang J Chen X Y Gu Y *et al*. Optimization of growth temperatures for InAlAs metamorphic buffers and high indium InGaAs on InP substrate J. *J. Infrared Millim. Waves* 2018 **37**(6): 699-703.

19 Zhu Y Chen X Y Ma Y J *et al*. Surface and optical properties of silicon nitride deposited by inductively coupled plasma-chemical vapor deposition J. *J. Semicond.* 2018 **39**(8): 083005.

20 Saha S Cassidy D T Thompson D A. Investigation of cross-hatch in In$_{0.3}$Ga$_{0.7}$As pseudo-substrates J. *J. Appl. Phys.* 2013 **113** (12): 5.

21 Xi S P Gu Y Zhang Y G *et al*. Effects of continuously graded or step-graded In$_x$Al$_{1-x}$As buffer on the performance of InP-based In$_{0.83}$Ga$_{0.17}$As photodetectors J. *J. Cryst. Growth* 2015 **425**: 337-340.

22 Shen W Z Shen S C Tang W G *et al*. Photoluminescence of quaternary GaInAsSb/AlGaAsSb strained multiple quantum wells J. *J. Appl. Phys.* 1995 **78**(9): 5696-5700.

23 Lei H P Wu H Z Lao Y F *et al*. Difference of luminescent properties between strained InAsP/InP and strain-compensated InAsP/InGaAsP MQWs J. *J. Cryst. Growth* 2003 **256**(1-2): 96-102.

24 Gu Y Zhang Y G Li A Z *et al*. Structural and Photoluminescence Properties for Highly Strain-Compensated InGaAs/InAlAs Superlattice J. *Chin. Phys. Lett.* 2009 **26**(7): 4.

25 Zhang Y G Xi S P Zhou L *et al*. Correction of intensity of emission spectra in a wide wave number range measured by FTIR J. *J. Infrared Millim. Waves* 2016 **35**(1): 63-67.

26 Gu Y Zhou L Zhang Y G *et al*. Dark current suppression in metamorphic In$_{0.83}$Ga$_{0.17}$As photodetectors with In$_{0.66}$Ga$_{0.34}$As/InAs superlattice electron barrier J. *Appl. Phys. Express* 2015 **8**(2): 022202.